Electronic Supplementary Information

All-in-One Polarized Cd/CdS/Halloysite Ferroelectric Hybrid for Exceptional Photocatalytic Hydrogen Evolution

Sen Lin, [a] Shutao Li, [a] Yihe Zhang, *[a] Tianyi Ma *[b] and Hongwei Huang *[a]

a. Beijing Key Laboratory of Materials Utilization of Nonmetallic Minerals and Solid Wastes, National Laboratory of Mineral Materials, School of Materials Science and Technology, China University of Geosciences, Beijing 100083, China.

b. Centre for Translational Atomaterials, Swinburne University of Technology, Hawthorn, VIC 3122, Australia.

Content

evolution reactions.

Figure S19: Digital photographs of (a) glass reactor, (b) 300 W xenon lamp with the model of PLS-SXE300C and (c) gas chromatography for H_2 evolution system.

Figure S20: DRS of CdS and P-CdS.

Figure S21: Nyquist plots of electrochemical impedance and enlarged view of (a) CdS, (b) CdS/HNTs-10, (c) Cd/CdS/HNTs-10 and (d) P-Cd/CdS/HNTs-10.

Figure S22: Time-resolved fluorescence spectra of CdS, CdS/HNTs-10 and P-Cd/CdS/HNTs-10.

Figure S23: Ferroelectric hysteresis loops of CdS at the frequency of 100 Hz with varieties of electric fields.

Figure S24: (a) Amplitude butterfly curve and (b) phase hysteresis loop of CdS obtained by PFM.

Figure S25: 3D images of (a) ferroelectric potential distribution and (b) surface ferroelectric potential of CdS obtained by SKPFM.

Figure S26: 3D images of (a) ferroelectric potential distribution and (b) surface ferroelectric potential of Pt-deposited P-Cd/CdS/HNTs-10 after H_2 evolution reactions obtained by SKPFM.

Table S1: Crystal lattice parameters of CdS, P-CdS and P-Cd/CdS.

Table S2: Typical wavenumber determined from FTIR spectra.

Table S3: Specific surface areas and porous parameters of HNTs, CdS and P-Cd/CdS/HNTs-10.

Table S4: Comparison of CdS-based photocatalysts on H_2 evolution performance.

Table S5: The AQE of P-Cd/CdS/HNTs-10 under visible light irradiation ($\lambda \geq 420$ nm) with different bandpass filters.

Figure S1. Digital photographs of HNTs, CdS and the series of CdS/HNTs-X.

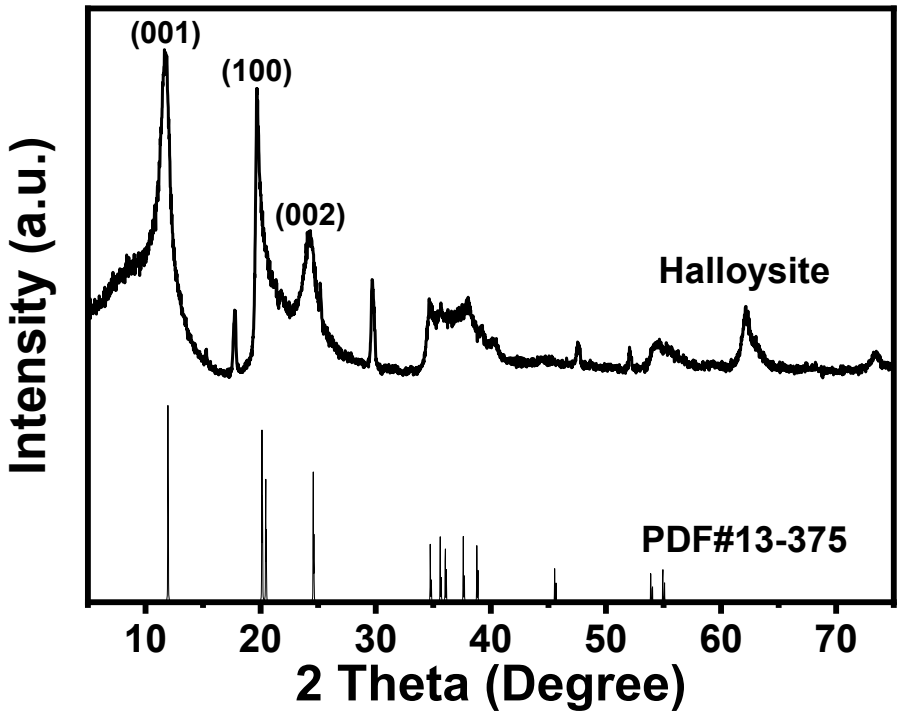

Figure S2. XRD pattern of HNTs.

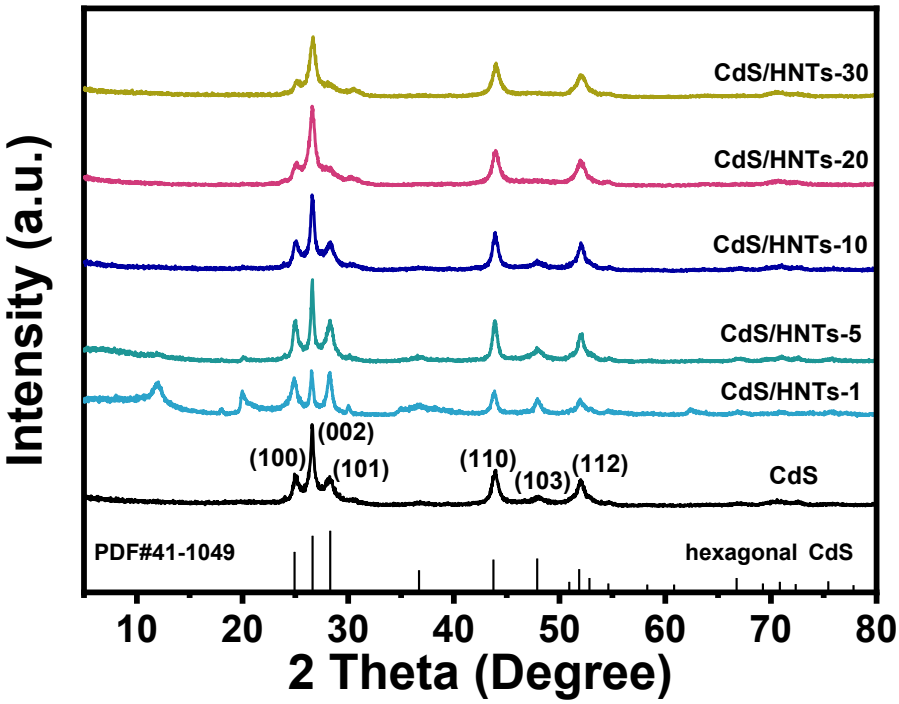

Figure S3. XRD patterns of CdS and the series of CdS/HNTs-X.

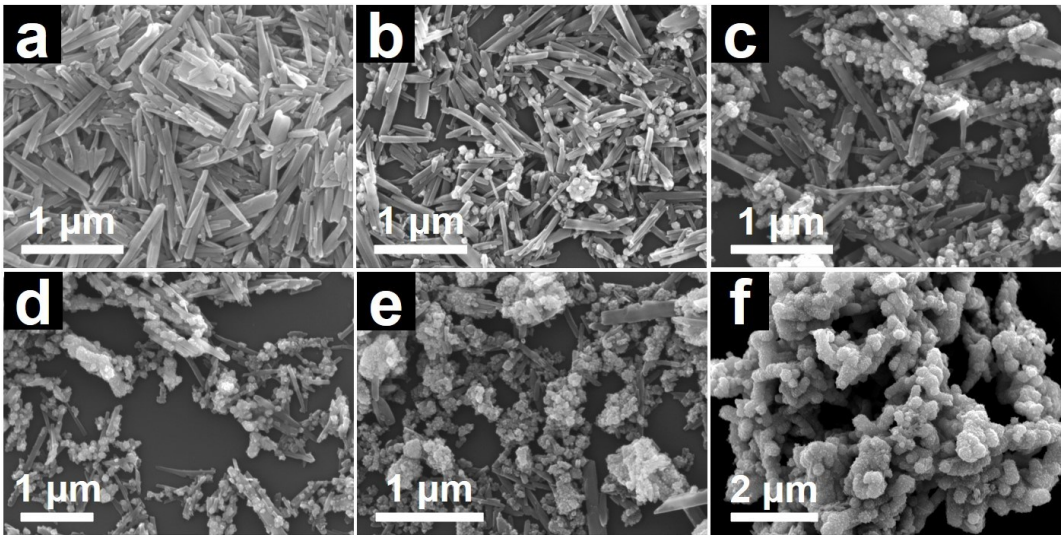

Figure S4. SEM images of (a) HNTs, (b) CdS/HNTs-1, (c) CdS/HNTs-5, (d) CdS/HNTs-10, (e) CdS/HNTs-20 and (f) CdS/HNTs-30.

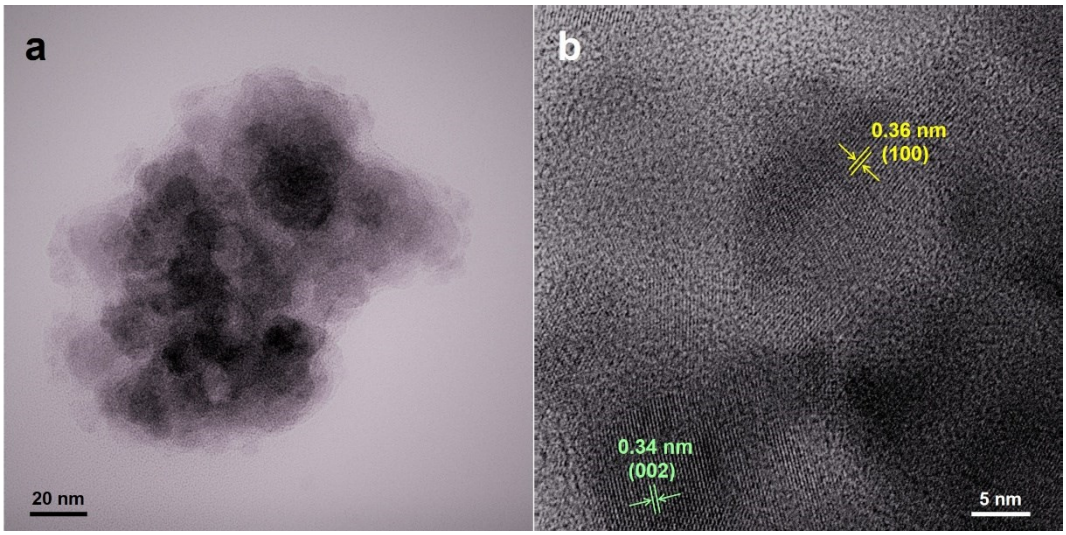

Figure S5. TEM image (a) and relevant high-resolution TEM image (b) of CdS nanospheres.

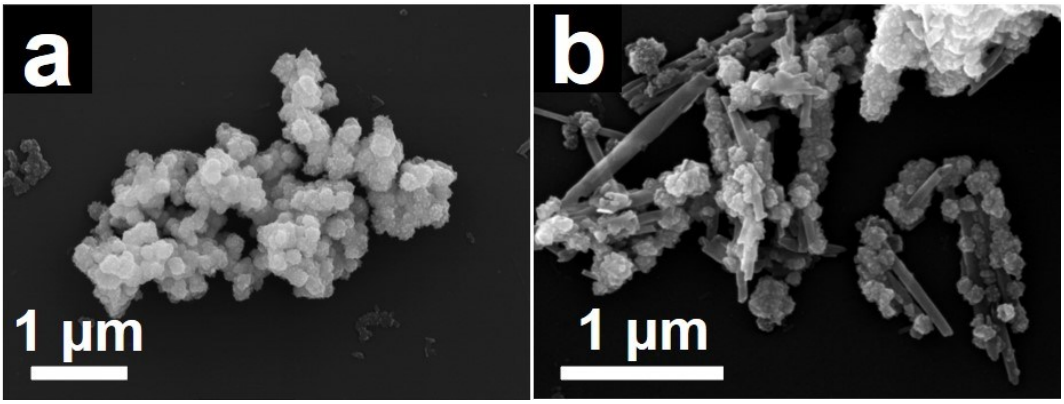

Figure S6. SEM images of (a) P-Cd/CdS and (b) P-Cd/CdS/HNTs-10.

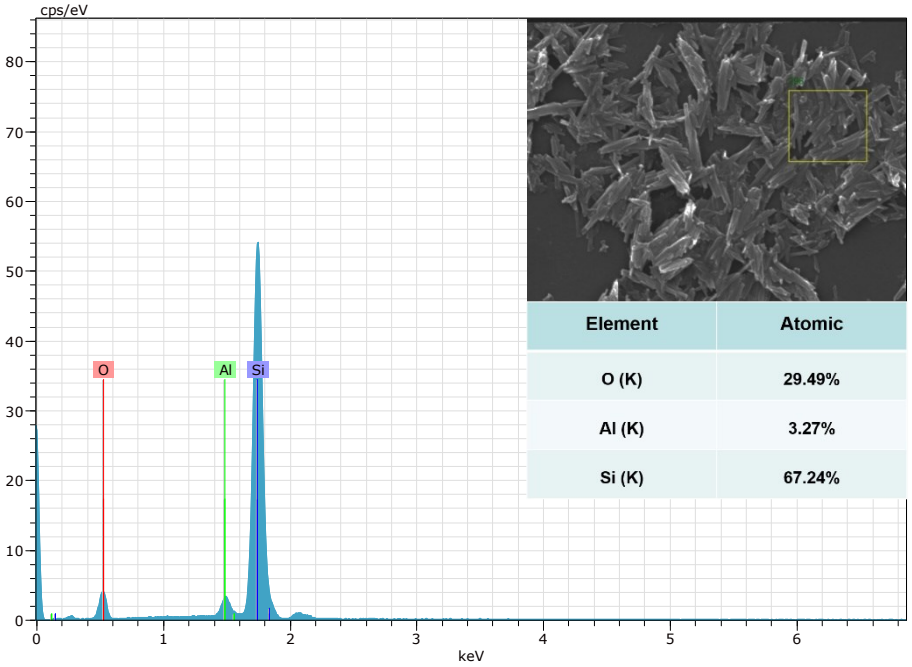

Figure S7. SEM and EDS images of HNTs.

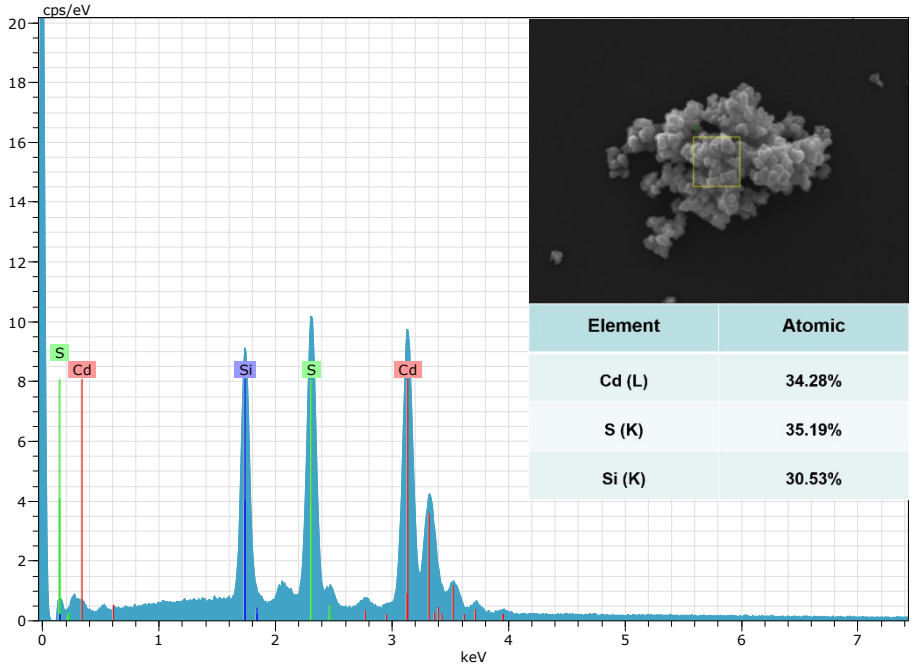

Figure S8. SEM and EDS images of CdS.

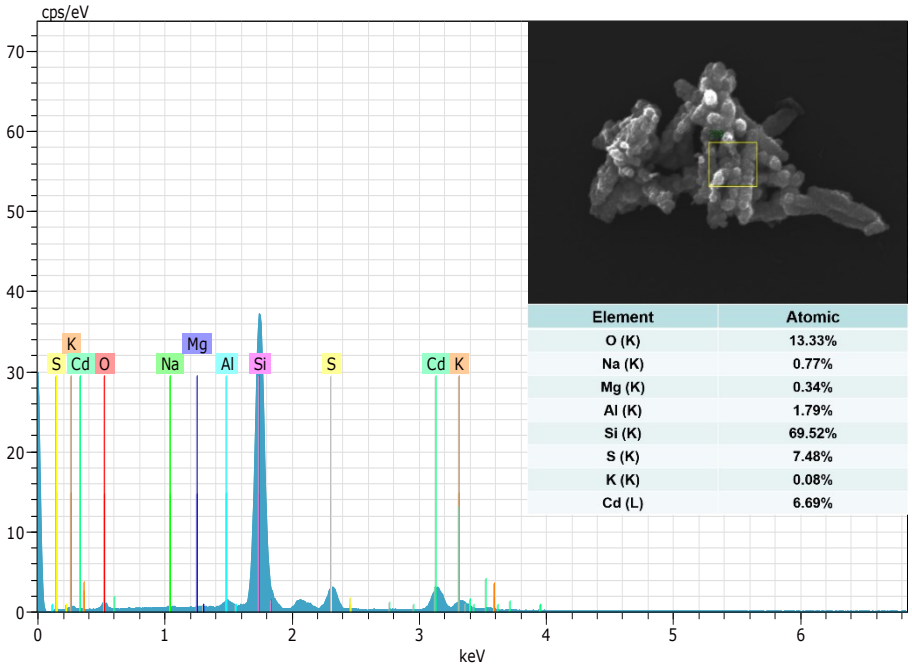

Figure S9. SEM and EDS images of CdS/HNTs-10.

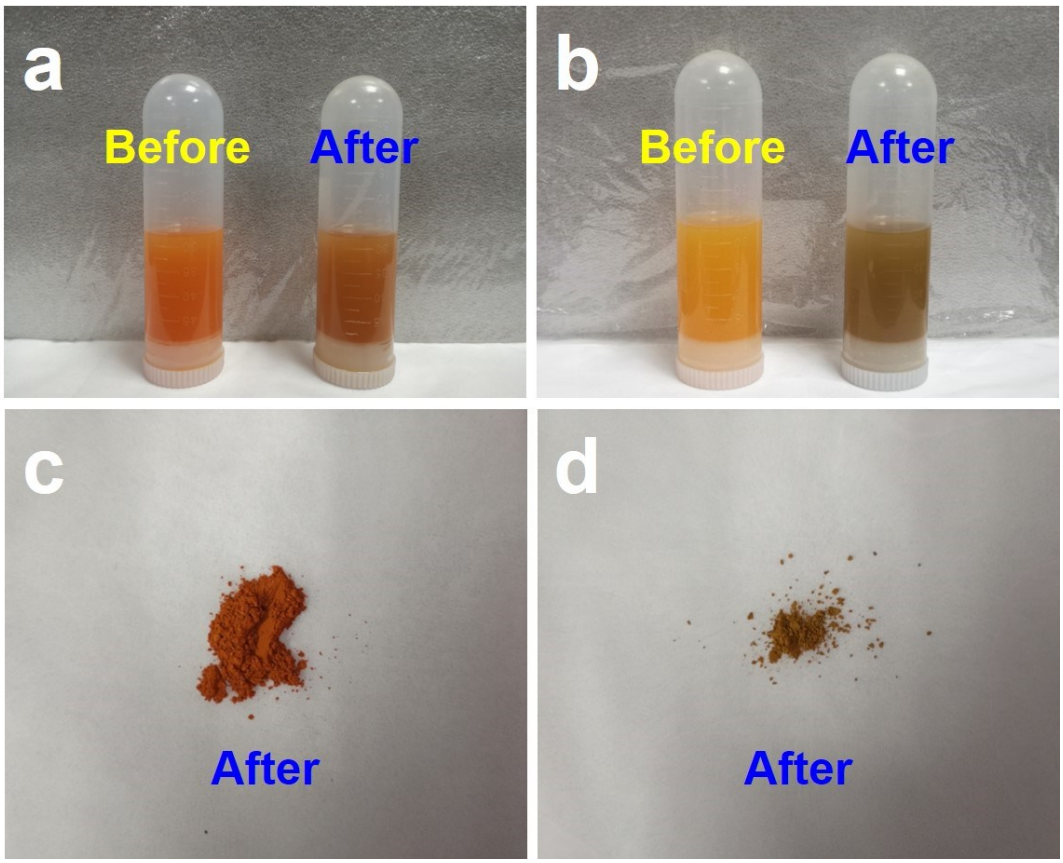

Figure S10. Digital photographs of (a, c) CdS and (b, d) CdS/HNTs-10 before and after reducton reactions.

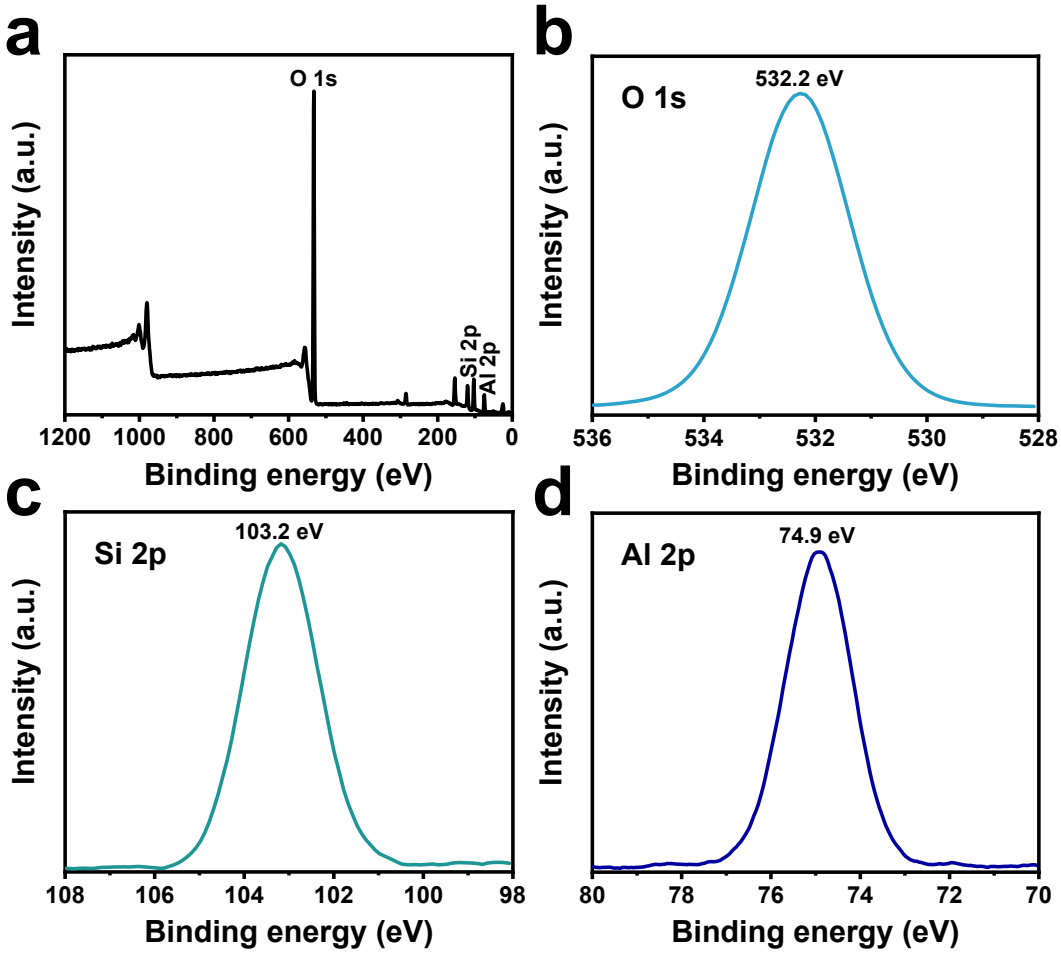

Figure S11. (a) XPS survey spectrum, high-resolution XPS spectra of (b) O, (c) Si and (d) Al for HNTs.

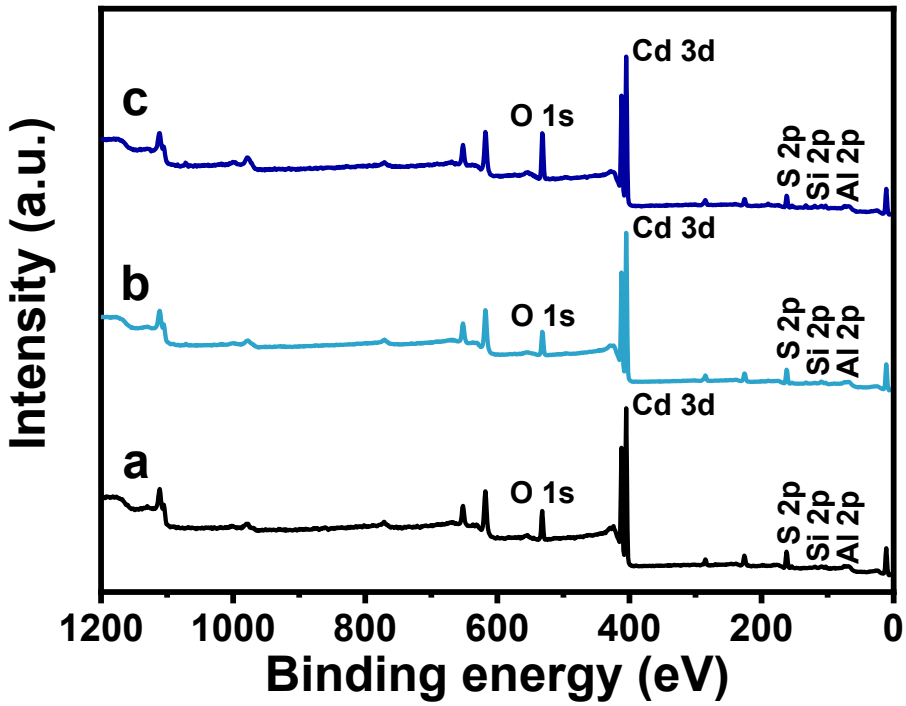

Figure S12. XPS survey spectra for (a) CdS/HNTs-10, (b) Cd/CdS/HNTs-10 and (c) P-Cd/CdS/HNTs-10.

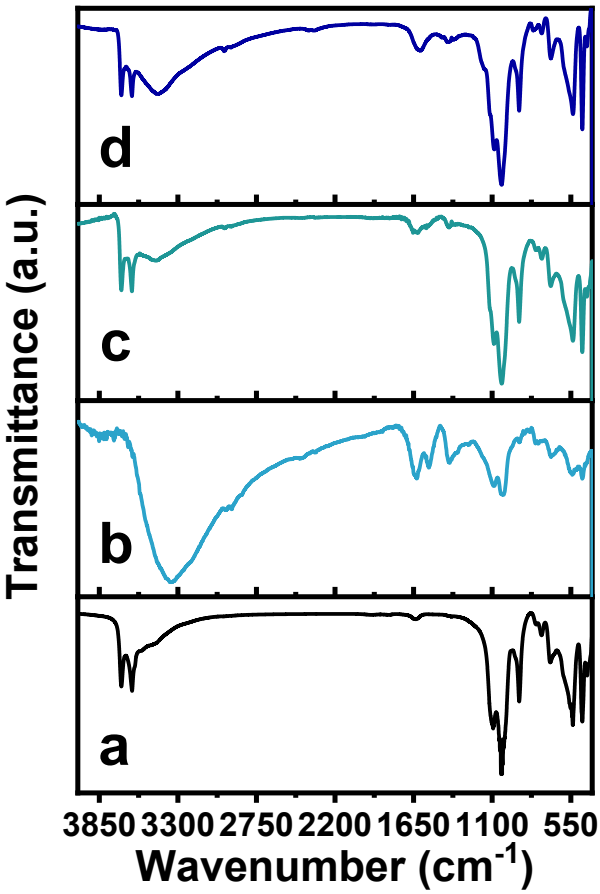

271

272 **Figure S13**. FTIR spectra of (a) HNTs, (b) CdS, (c) CdS/HNTs-10 and (d) P-

273 Cd/CdS/HNTs-10.

274

275

276

277

278

279

280

281

282

283

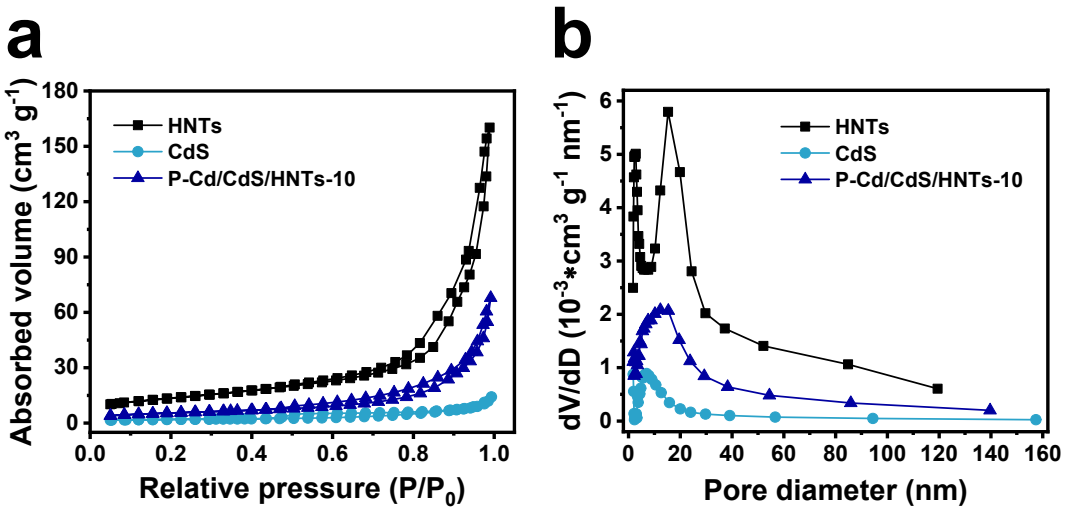

Figure S14. (a) Nitrogen adsorption-desorption isotherms and (b) pore size distributions of HNTs, CdS and P-Cd/CdS/HNTs-10.

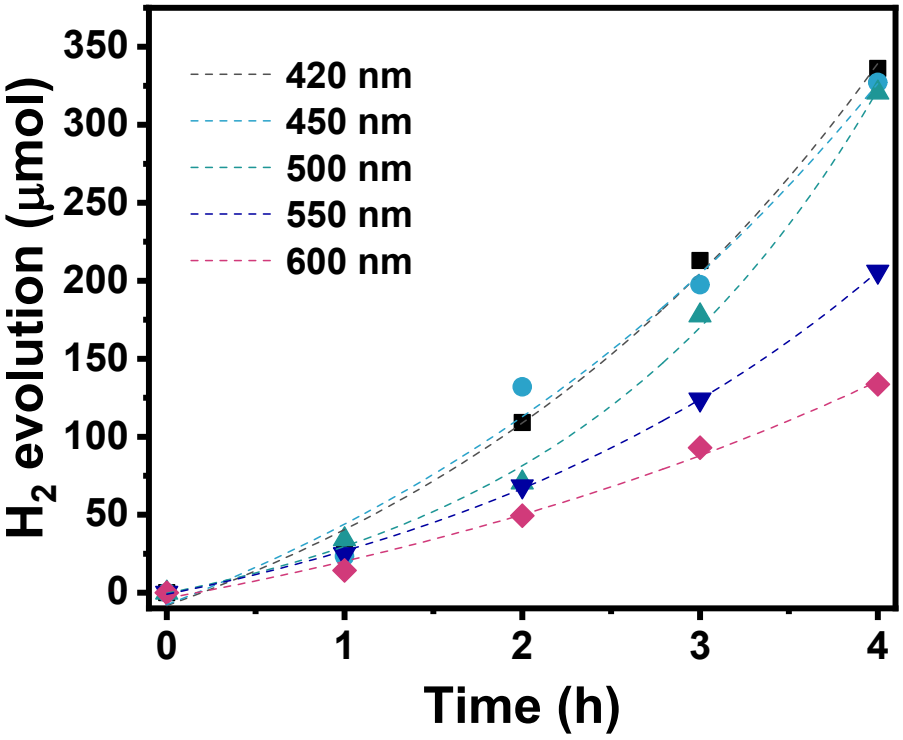

Figure S15. Time courses of H_2 evolution for Pt-deposited P-Cd/CdS/HNTs-10 under visible light irradiation ($\lambda \geq 420$ nm) with different bandpass filters.

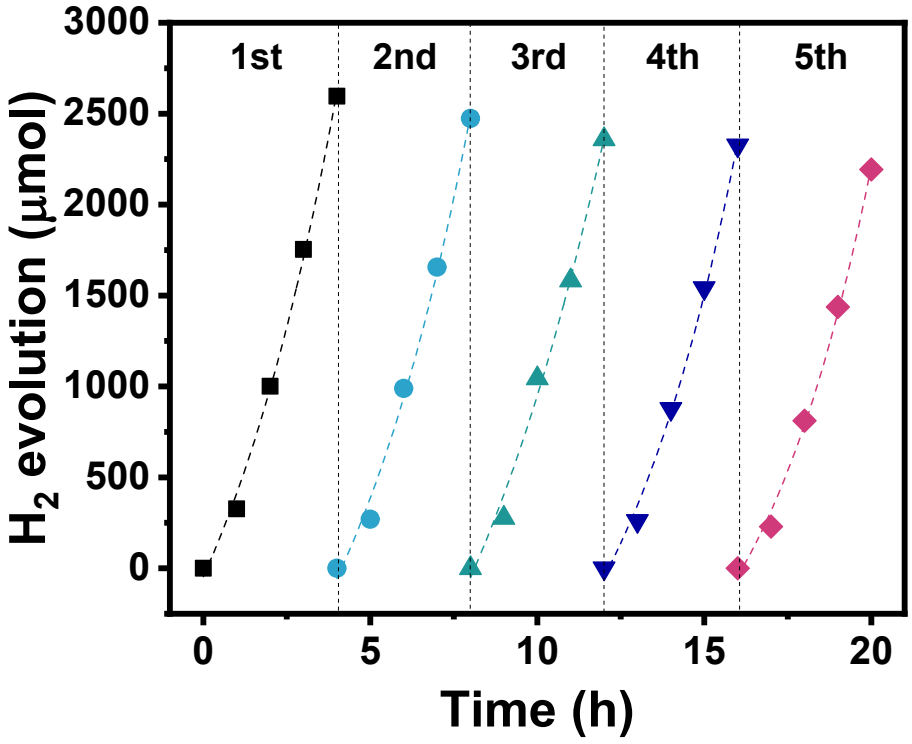

Figure S16. Stability of H_2 evolution for Pt-deposited P-Cd/CdS/HNTs-10.

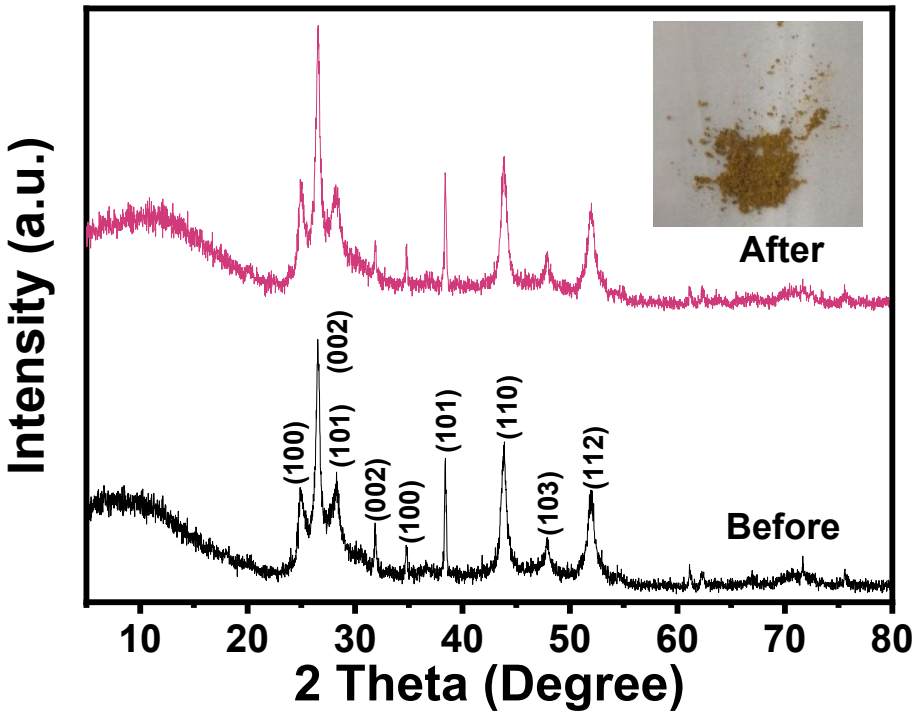

Figure S17. XRD patterns of Pt-deposited P-Cd/CdS/HNTs-10 before and after H_2 evolution reactions (inset is the relevant digital photograph of sample after reactions).

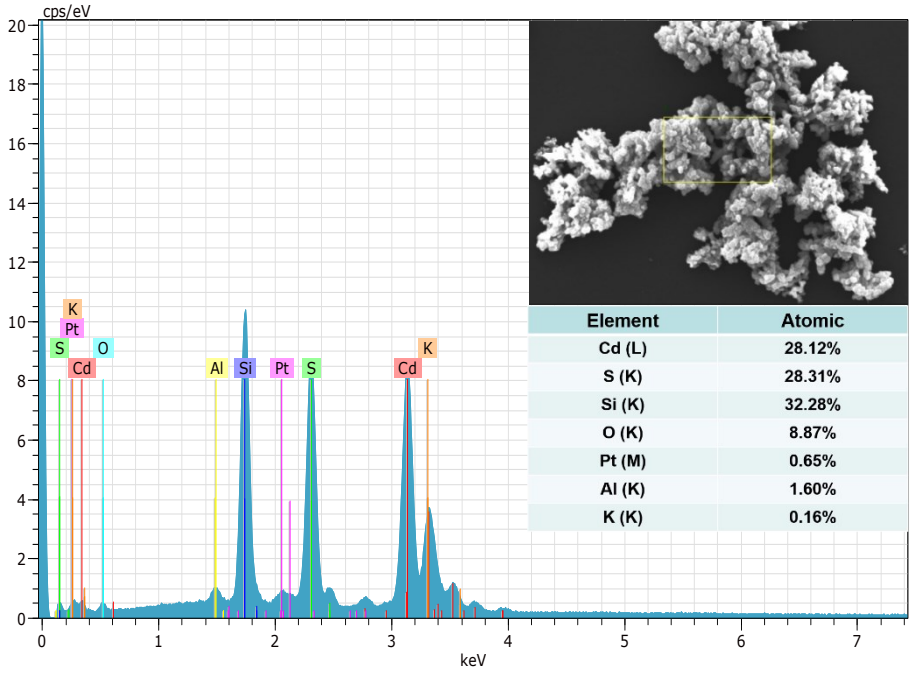

Figure S18. SEM and EDS images of Pt-deposited P-Cd/CdS/HNTs-10 after H_2 evolution reactions.

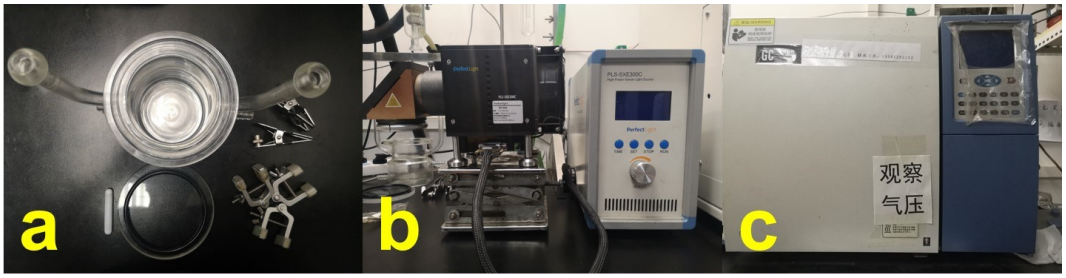

Figure S19. Digital photographs of (a) glass reactor, (b) 300 W xenon lamp with the model of PLS-SXE300C and (c) gas chromatography for H_2 evolution system.

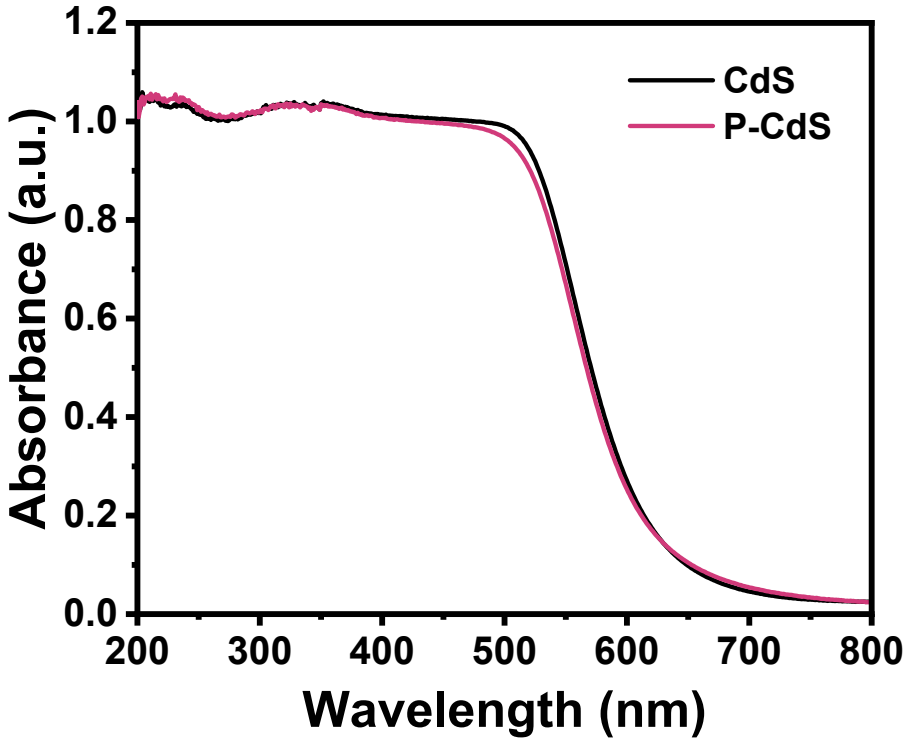

Figure S20. DRS of CdS and P-CdS.

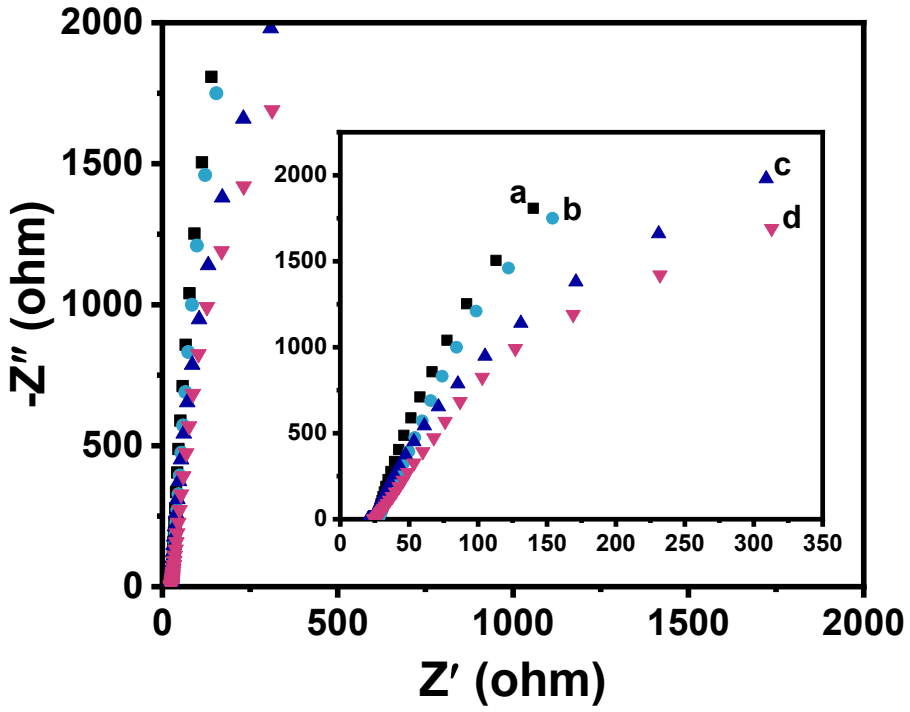

394

395 **Figure S21**. Nyquist plots of electrochemical impedance and enlarged view of (a)
396 CdS, (b) CdS/HNTs-10, (c) Cd/CdS/HNTs-10 and (d) P-Cd/CdS/HNTs-10.

397

398 **Note**: The electrochemical impedance spectra (EIS) indicated that the arc radius of
399 Nyquist plots for P-Cd/CdS/HNTs-10 is the smallest, suggesting a lower interfacial
400 resistance and a faster charge migration efficiency occurred on P-Cd/CdS/HNTs-10
401 compared with other samples.

402

403

404

405

406

407

408

409

410

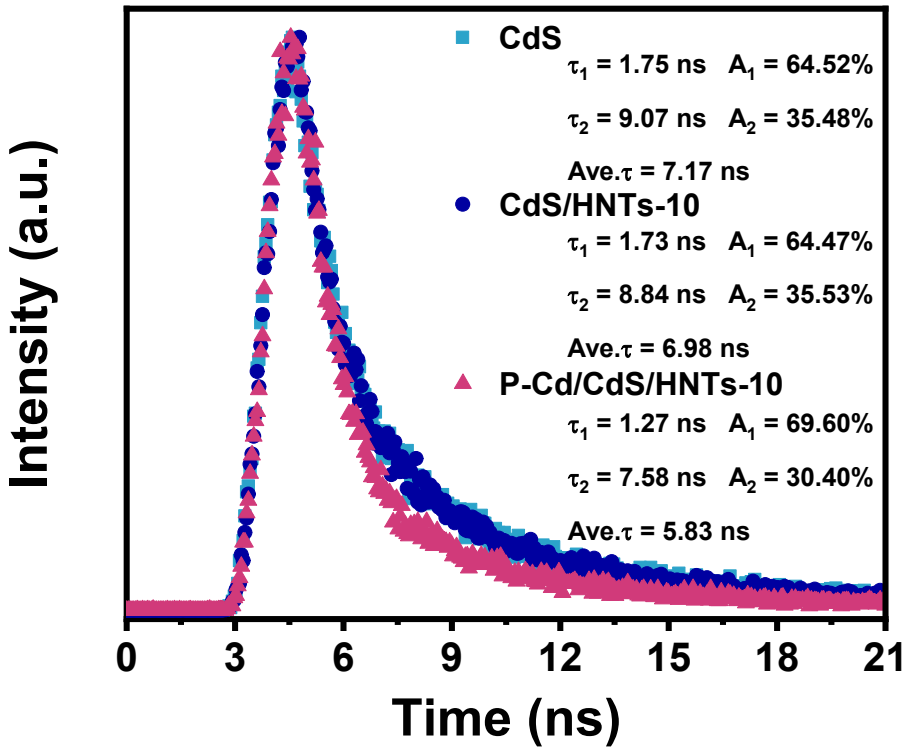

411

412 **Figure S22**. Time-resolved fluorescence spectra of CdS, CdS/HNTs-10 and P-
413 Cd/CdS/HNTs-10.

414

415 **Note**: The photoinduced charge migration dynamics of as-synthesized materials were
416 investigated by ns-level time-resolved transient photoluminescence (TRPL) decay,
417 and the radiative lifetime fitting consequences were inserted. It was shown that
418 double-exponential curves were fitted to the decay profiles. The average lifetime (τ_A)
419 of P-Cd/CdS/HNTs-10 was 5.83 ns and relatively faster than CdS/HNTs-10 (6.98 ns)
420 and CdS (7.17 ns), indicating that the photogenerated charge carriers of P-
421 Cd/CdS/HNTs-10 could be availably separated by the enhanced intrinsic spontaneous
422 polarization electric field and easier to be captured by the cadmium defect sites, which
423 favored the photocatalytic activity. The average fluorescence lifetime is calculated as
424 follows:

$$\tau_A = \frac{A_1\tau_1^2 + A_2\tau_2^2}{A_1\tau_1 + A_2\tau_2}$$

where A_1 and A_2 are the magnitudes, τ_1 and τ_2 are the lifetimes.[1]

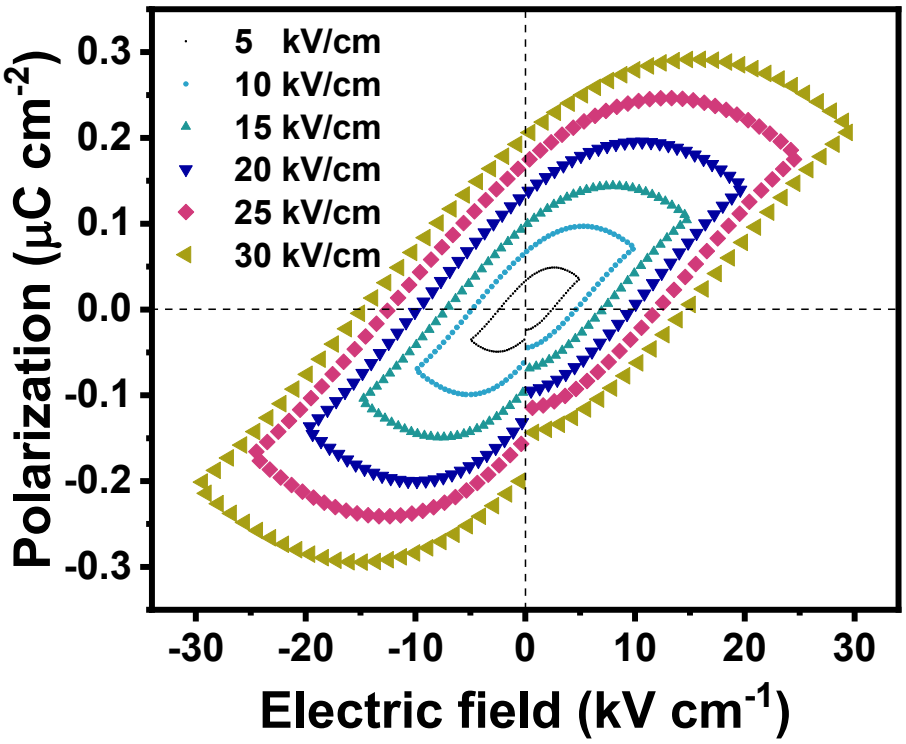

Figure S23. Ferroelectric hysteresis loops of CdS at the frequency of 100 Hz with varieties of electric fields.

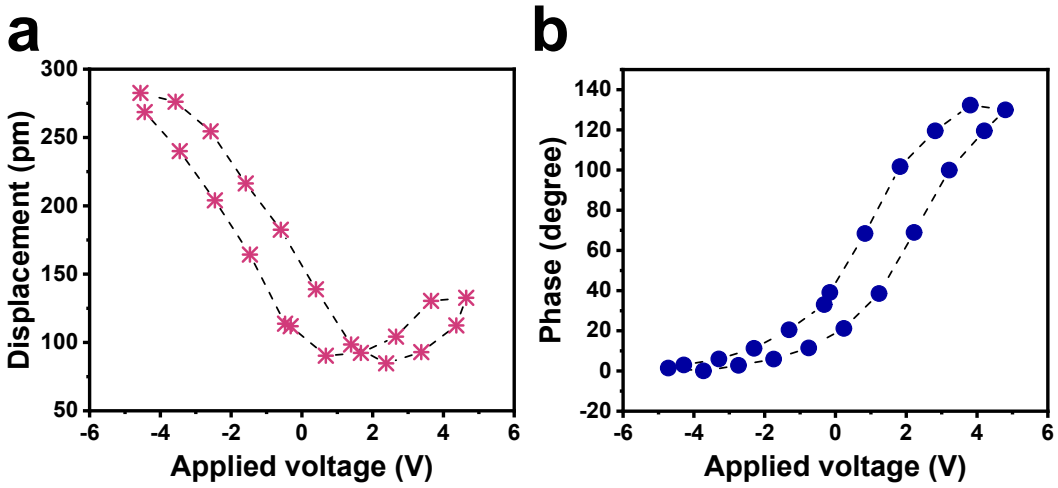

Figure S24. (a) Amplitude butterfly curve and (b) phase hysteresis loop of CdS obtained by PFM.

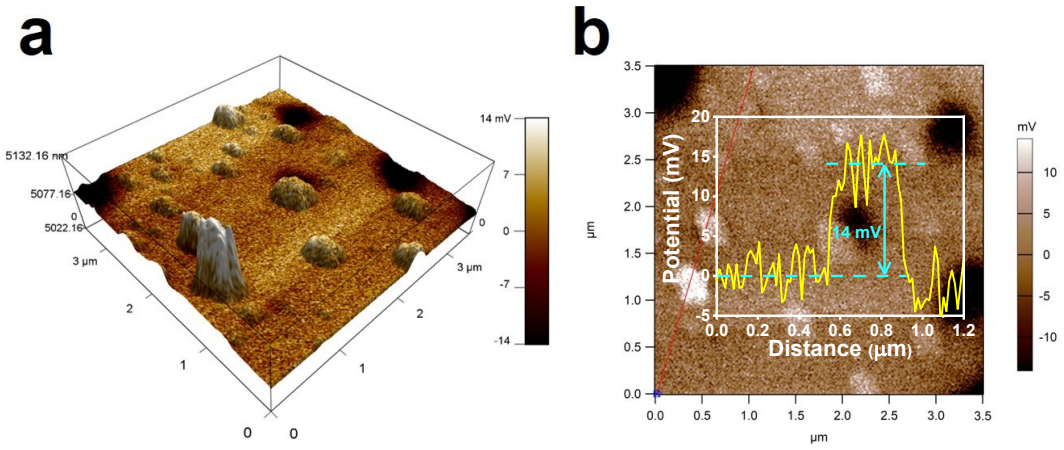

Figure S25. 3D images of (a) ferroelectric potential distribution and (b) surface ferroelectric potential of CdS obtained by SKPFM.

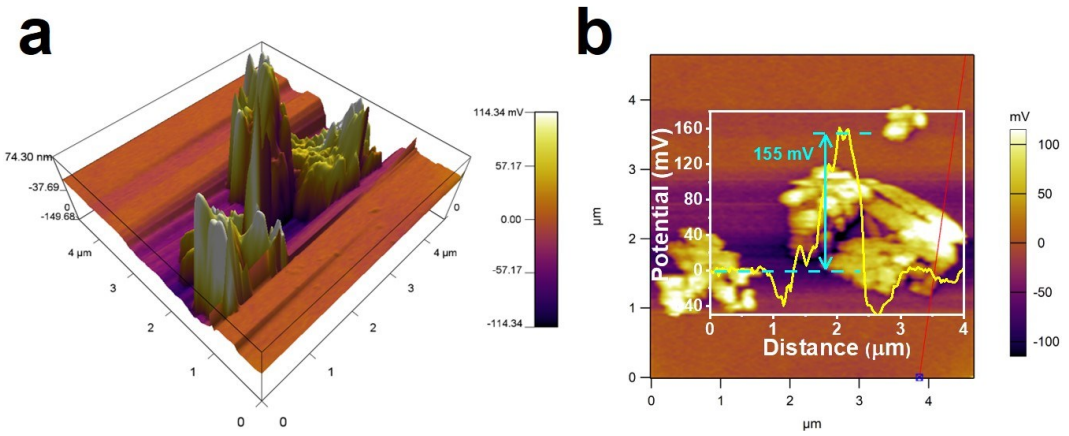

Figure S26. 3D images of (a) ferroelectric potential distribution and (b) surface ferroelectric potential of Pt-deposited P-Cd/CdS/HNTs-10 after the cycling H_2 evolution reactions obtained by SKPFM.

Table S1. Crystal lattice parameters of CdS, P-CdS and P-Cd/CdS.

Sample	*a* (Å)	*b* (Å)	*c* (Å)
CdS	4.123	4.123	6.709
P-CdS	4.122	4.122	6.711
P-Cd/CdS	4.122	4.122	6.711

540

541 **Table S2**. Typical wavenumber determined from FTIR spectra.

a	3695.4 cm^{-1} O−H stretching	3620.3 cm^{-1} O−H stretching	1093.2 cm^{-1} Si−O−Si antisymmetric stretching	910.9 cm^{-1} Al−OH in-plane bending	694.3 cm^{-1} CO_3^{2-} in-plane bending
b	3386.1 cm^{-1} $-NH_2$ antisymmetric stretching 1020.8 cm^{-1} C＝S stretching	1627.2 cm^{-1} $-NH_2$ variance angle 689.7 cm^{-1} CO_3^{2-} in-plane bending	1543.7 cm^{-1} −COO antisymmetric stretching	1398.2 cm^{-1} −COO symmetric stretching	1090.0 cm^{-1} C＝S stretching
c	3695.2 cm^{-1} O−H stretching 911.4 cm^{-1} Al−OH in-plane bending	3621.4 cm^{-1} O−H stretching 690.0 cm^{-1} CO_3^{2-} in-plane bending	3454.3 cm^{-1} $-NH_2$ antisymmetric stretching	1654.2 cm^{-1} $-NH_2$ variance angle	1086.6 cm^{-1} C＝S stretching
d	3695.4 cm^{-1} O−H stretching 911.3 cm^{-1} Al−OH in-plane	3621.1 cm^{-1} O−H stretching 689.4 cm^{-1} CO_3^{2-} in-plane	3442.1 cm^{-1} $-NH_2$ antisymmetric stretching	1602.2 cm^{-1} $-NH_2$ variance angle	1085.5 cm^{-1} C＝S stretching

	bending	bending

Table S3. Specific surface areas and porous parameters of HNTs, CdS and P-Cd/CdS/HNTs-10.

Sample	Surface area ($m^2 g^{-1}$)	Pore volume ($cm^3 g^{-1}$)	Average pore size (nm)
HNTs	47.52	0.25	20.42
CdS	6.47	0.02	12.40
P-Cd/CdS/HNTs-10	18.99	0.10	20.41

560

561 **Table S4**. Comparison of CdS-based photocatalysts on H_2 evolution performance.

Photocatalyst	Sacrificial agent	Light source	Incident light	Activity (mmol g^{-1} h^{-1})	Ref.
P-Cd/CdS/HNTs-10	Lactic acid	300W Xe	≥ 420 nm	32.11	This work
CdS/CoS_2	Ascorbic acid	CEL-S500	Solar light	5.54	[1]
CdS	Na_2S-Na_2SO_3	300W Xe	≥ 420 nm	24.33	[2]
CdS/Halloysite	Na_2S-Na_2SO_3	30W LED	≥ 450 nm	20.10	[3]
NiCd/CdS	Na_2S-Na_2SO_3	300W Xe	≥ 410 nm	11.57	[4]
MoS_2/CdS	Lactic acid	300W Xe	≥ 420 nm	60.28	[5]
TiO_2/CdS	Na_2S-Na_2SO_3	300W Xe	≥ 420 nm	19.92	[6]
CdS@ZnO	Na_2S-Na_2SO_3	225W Xe	Solar light	71.39	[7]
CDs/CdS[a)]	Lactic acid	300W Xe	Solar light	6.70	[8]
In_2O_3/Au/CdS	Na_2S-Na_2SO_3	225W Xe	Solar light	1.72	[9]
MXene@Au@CdS	Na_2S-Na_2SO_3	300W Xe	≥ 420 nm	17.07	[10]
CdS@Zn-C[b)]	Na_2S-Na_2SO_3	20W LED	≥ 420 nm	6.60	[11]
CdS@G@TiO_2[c)]	Na_2S-Na_2SO_3	150W Xe	Solar light	1.51	[12]
$ZnIn_2S_4$-MoS_2/CdS	Triethanolamine	300W Xe	≥ 420 nm	7.57	[13]
CdS-$Cu_{2-x}S$/MoS_2	Na_2S-Na_2SO_3	300W Xe	≥ 400 nm	14.18	[14]

562

563 **Note**: [a)]CDs = Carbon dots; [b)]C = Carbon layer; [c)]G = Graphene

564

565

566

567

Table S5. The AQE of P-Cd/CdS/HNTs-10 under visible light irradiation ($\lambda \geq 420$ nm) with different bandpass filters.

Light wavelength (nm)	**AQE (%)**
420	45.13
450	39.66
500	29.94
550	16.39
600	9.72

References

1 P. F. Wang, Y. S. Mao, L. N. Li, Z. R. Shen, X. Luo, K. F. Wu, P. F. An, H. T. Wang, L. N. Su, Y. L, S. H. Zhan, *Angew. Chem., Int. Ed*, 2019, **131**, 11451.

2 X. Q. Hao, Y. Hu, Z. W. Cui, J. Zhou, Y. Wang, Z. G. Zou, *Appl. Catal., B*, 2019, **244**, 694.

3 V. Vinokurov, A. V. Stavitskaya, E. V. Ivanov, P. A. Gushchin, D. V. Kozlov, A. Y. Kurenkova, P. A. Kolinko, E. A. Kozlova, Y. M. Lvov, *ACS Sustainable Chem. Eng*, 2017, **5**, 11316.

4 B. Wang, S. He, L. L. Zhang, X. Y. Huang, F. Gao, W. H. Feng, P. Liu, *Appl. Catal., B*, 2018, **243**, 229.

5 X. L. Yin, G. Y. He, B. Sun, W. J. Jiang, D. J. Xue, A. D. Xia, L. J. Wan, J. S. Hu, *Nano Energy*, 2016, **28**, 319.

6 Y. Huang, J. Chen, W. Zou, L. X. Zhang, L. Hu, M. He, L. Gu, J. X. Deng, X. R. Xing, *Dalton Trans*, 2016, **45**, 1160.

7 D. D. Ma, J. W. Shi, Y. J. Zou, Z. Y. Fan, X. Ji, C. M. Niu, L. Z. Wang, *Nano Energy*, 2017, **39**, 183.

8 C. Zhu, C. Liu, Y. J. Fu, J. Gao, H. Huang, Y. Liu, Z. H. Kang, *Appl. Catal., B*, 2018, **242**, 178.

9 D. D. Ma, J. W. Shi, D. K. Sun, Y. J. Zou, L. H. Cheng, C. He, Z. Y. Wang, C. M. Niu, *ACS Sustainable Chem. Eng*, 2019, **7**, 547.

10 J. J. Yin, F. K. Zhan, T. F. Jiao, W. H. Wang, G. C. Zhang, J. H. Jiao, G. Y. Jiang, Q. R. Zhang, J. M. Gu, Q. M. Peng, *Sci. China Mater*, 2020, 1.

11 Y. Shi, X. F. Lei, L. G. Xia, Q. Wu, W. F. Yao, *Chem. Eng. J*, 2020, **393**, 124751.

12 M. Zubair, I. H. Svenum, M. Rnning, J. Yang, *Catalysts*, 2020, **10**, 358.

13 L. Wang, H. H. Zhou, H. Z. Zhang, Y. L. Song, H. Zhang, L. K. Luo, Y. F. Yang, S. Q. Bai, Y. Wang, S. X. Liu, *Nanoscale*, 2020, **12**, 13791.

14 G. N. Liu, C. Kolodziej, R. Jin, S. P. Qi, Y. B. Lou, J. X. Chen, D. C. Jiang, Y. X. Zhao, C. Burda, *ACS nano*, 2020, **14**, 5468.